PAPER

Effect of structural optimization on the photovoltaic performance of dithieno[3,2-*b*:2′,3′-*d*]pyrrole-based dye-sensitized solar cells†

Hai Zhang, [ID] *[a] Zafar Iqbal,[b] Zhen-E. Chen[a] and Yan-Ping Hong[c]

Five novel organic push–pull dyes, **DT**, **CD-T**, **TD-T**, **CD-C** and **TD-P**, based on carbazole or triphenylamine as donors, dithieno[3,2-*b*:2′,3′-*d*]pyrrole as a π-spacer and cyanoacetic acid as an acceptor were synthesized, and their structures were optimized for DSSCs. Dithieno[3,2-*b*:2′,3′-*d*]pyrrole was linked with either carbazole or triphenylamine *via* a Suzuki coupling reaction. Followed by formylation *via* a Vilsmeier–Haak reaction, and then a Knoevenagel condensation reaction was employed to link cyanoacetic acid, producing the carbazole-based dyes **CD-C** and **CD-T** and the triphenylamine-based dyes **TD-P** and **TD-T**. Meanwhile, the dye **DT** was synthesized as a reference for comparison. The molar extinction coefficients of the carbazole-based dyes **CD-T** and **CD-C** were 56 370 M^{-1} cm^{-1} and 62 471 M^{-1} cm^{-1}, while those of the dyes based on triphenylamine, **TD-T** and **TD-P**, were 44 555 M^{-1} cm^{-1} and 49 945 M^{-1} cm^{-1}, respectively. The optimized power conversion efficiency of **CD-T** reached 6.63% with an open-circuit voltage of 710 mV, a short-circuit current density of 14.55 mV cm^{-2}, and a fill factor of 0.64.

1. Introduction

Dye-sensitized solar cells (DSSCs) based on nanocrystalline thin films have been extensively studied by various research groups around the world since 1991 (ref. 1) and have shown great progress in three major areas: efficiency, stability and the mechanism.[2] Improving the photovoltaic properties of dye-sensitized solar cells involves systematic studies, with the most important projects focusing on the improvement of nanocrystalline semiconductor films, photosensitizing dyes and electrolytes. As one of the most important components of a DSSC, the sensitizer has been a hotspot for researchers. Through the structural modification of sensitizers, the spectral response of DSSCs can be broadened, and the photoelectric conversion efficiency and stability can be improved.[3–5] At present, photosensitized dyes in DSSCs mainly contain ruthenium complexes, zinc porphyrins, phthalocyanins, metal-free organic dyes, and so on.[6–14] Metal-free dyes have been extensively investigated and have shown record power conversion efficiencies of over 14% under AM 1.5 G irradiation.[15] However, due to the high cost and limited resources associated with

ruthenium dyes, the prospects for metal-free organic dyes will be very broad once adequate stability and efficiency have been achieved. Metal-free organic dyes began to receive more attention around the year 2000. Since 2001, large numbers of donor groups, acceptor groups and conjugated units connecting them have been combined in various ways, resulting in a wide variety of metal-free organic dyes.[16–32]

In general, the most effective means to enhance efficiency is to enhance the photocurrent and photovoltaic voltage. The efficiency of photocurrent generation is related to three factors: light capture efficiency, electron injection efficiency and electron collection efficiency. DSSCs have high light-trapping efficiency, which means that the absorption spectrum is broad and the absorbance is large. The former is related to the light absorption width of the dye, and the latter is determined by the molar extinction coefficient and light adsorption amount of the dye.[33] Absorption in the visible region mainly occurs due to intra-molecular charge transfer (ICT) transition in dyes, and the basis for this transition is the existence of a molecular electronic push–pull effect. The electron donor and acceptor in a D–π–A dye act as a push–pull electron system; the stronger the push–pull electron effect, the more obvious the ICT effect and the more the corresponding absorption band is red-shifted. On the other hand, the molar extinction coefficient and molecular structure have a very close relationship. Grätzel *et al.* achieved remarkable results by optimizing the molecular structure to increase the molar extinction coefficient of metal ruthenium dyes.[34] It has been reported that changing the length of the conjugated chains and the twist angle are very important in improving the molar extinction coefficient. A planar conjugated

[a]School of Chemistry and Chemical Engineering, Qianbei Featured Resources Applied Research Key Laboratory, Zunyi Normal College, Zunyi 563006, Guizhou, China. E-mail: haizhang@vip.sina.com; Fax: +86 0851 28927159; Tel: +86 0851 28927159

[b]Applied Chemistry Research Centre, PCSIR Laboratories Complex, Feroze pur Road, Lahore 54000, Pakistan

[c]Jiangxi Key Laboratory of Natural Product and Functional Food, College of Food Science and Engineering, Jiangxi Agricultural University, Nanchang 330045, China

† Electronic supplementary information (ESI) available. See DOI: 10.1039/c7ra05716d

bridge structure can not only increase the degree of molecular conjugation, but can also effectively increase the molar extinction coefficient of the dye molecule. Undoubtedly, it is interesting to introduce a large planar conjugated π-bridge structure in the molecule to obtain dye molecules with high absorptivity in the visible and near-infrared regions.

Dithieno[3,2-*b*:20,30-*d*]pyrrole (**DTP**) has a completely flat crystal structure, which means that the introduction of **DTP** units can effectively improve conjugation, conductivity and charge carrier mobility. Combining a suitable donor group and acceptor group, **DTP**-based dyes have been shown to be excellent sensitizers for high efficiency DSSCs.[35–42] Triphenylamine has been widely used as the electron donor of sensitizers, due to its good electron donating and transporting capabilities. In addition, the nonplanar property of triphenylamine contributes to the reduction of dye aggregation and charge recombination. In contrast, as another common donor unit, the electron-donating ability of carbazole is relatively weaker than that of triphenylamine, and its spatial structure is almost planar, but it is more favorable for electron transport.

Taking all these factors into account, the current effort was made to find a well-suited structure for DSSCs. Towards this aim, we have designed and synthesized five novel organic dyes with **DTP** moieties. In this paper, a structure–performance relationship was studied, and in particular, the effect of different electron donors attached at different sites was explored. Furthermore, spectroscopic and electrochemical studies, theoretical calculations and *J*–*V* experiments were carried out. IPCE and electrochemical impedance spectroscopic analyses of the dyes **DT**, **CD-T**, **TD-T**, **CD-C** and **TD-P** were performed in detail. Efforts were also put forward to understand how subtle structural variations in the sensitizers affect the photovoltaic performance in DSSCs.

2. Materials and instruments

Dry THF and toluene were distilled over sodium/benzophenone. Other reagents were purchased from commercial sources and used without further purification. All glassware was dried under infrared, assembled hot, and cooled to room temperature in a desiccator. The transfer of liquids was done using standard syringe techniques, and all reactions were performed under a stream of dry argon. Reactions were monitored by using TLC, and chromatographic separations were performed using standard column methods with silica gel (300–400 mesh).

2.1. Synthesis of dyes

2.1.1. 4-[4-(Di-*p*-tolylamino)phenyl]-6-(9-octyl-9*H*-carbazol-3-yl)-4*H*-dithieno[3,2-*b*:2′,3′-*d*]pyrrole-2-carbaldehyde (4-T). A mixture of 9-octyl-3-(4,4,5,5-tetramethyl-1,3,2-dioxaborolan-2-yl)-9*H*-carbazole (219 mg, 0.54 mmol), **3-T** (150 mg, 0.27 mmol), tetrakis(triphenylphosphine)palladium(0) (30 mg, 0.026 mmol), and potassium carbonate (2 M aqueous solution 1 mL, 2 mmol) in THF (25 mL) was stirred and heated to reflux under argon for 20 h. The reaction mixture was poured into water and extracted with DCM, and the combined extracts were washed with brine,

dried over anhydrous MgSO$_4$, and filtered. The solvent was removed by rotary evaporation under vacuum, and the crude product was purified using column chromatography on silica gel to give a yellow solid in 68.7% (140 mg) yield. Mp 226–227 °C. ^{1}H NMR (CDCl$_3$, 400 MHz, ppm): δ 9.85 (s, 1H), 8.36 (d, *J* = 1.2 Hz, 1H), 8.15 (d, *J* = 8 Hz, 1H), 7.77–7.74 (m, 2H), 7.52–7.48 (m, 1H), 7.43–7.40 (m, 4H), 7.38 (s, 1H), 7.28–7.25 (m, 1H), 7.21–7.18 (m, 2H), 7.15–7.09 (m, 8H), 7.31 (t, *J* = 7.2 Hz, 2H), 2.35 (s, 6H), 1.92–1.85 (m, 2H), 1.41–1.24 (m, 10H), 0.88–0.84 (m, 3H). ^{13}C NMR (CDCl$_3$, 100 MHz): δ ppm 182.8, 149.6, 149.1, 147.4, 144.9, 143.1, 141.0, 140.5, 139.9, 133.3, 131.9, 130.2, 126.2, 125.8, 125.1, 125.0, 124.0, 123.4, 122.8, 122.7, 120.6, 119.3, 117.8, 114.6, 109.2, 109.0, 106.6, 43.3, 31.8, 29.4, 29.2, 29.0, 27.3, 22.6, 20.9, 14.1. HRMS (ESI, *m/z*): [M + H]$^+$ calcd for (C$_{49}$H$_{45}$N$_3$OS$_2$): 756.3077, found: 756.3070.

2.1.2. 4-Hexyl-6-(9-octyl-9*H*-carbazol-3-yl)-4*H*-dithieno[3,2-*b*:2′,3′-*d*]pyrrole-2-carbaldehyde (4-C). Compound **4-C** was synthesized from **3-C** according to the same procedure as that of **4-T**, and was obtained as an orange yellow solid in 91.9% yield. Mp 107–108 °C. ^{1}H NMR (CDCl$_3$, 400 MHz, ppm): δ 9.81 (s, 1H), 8.32–8.31 (m, 1H), 8.13 (d, *J* = 7.6 Hz, 1H), 7.73–7.70 (m, 1H), 7.54 (s, 1H), 7.50–7.47 (m, 1H), 7.41–7.35 (m, 2H), 7.28–7.25 (m, 1H), 7.19 (s, 1H), 4.25 (t, *J* = 7.2 Hz, 2H), 4.18 (t, *J* = 7.2 Hz, 2H), 1.91–1.84 (m, 4H), 1.33–1.23 (m, 16H), 0.89–0.84 (m, 6H). ^{13}C NMR (CDCl$_3$, 100 MHz): δ ppm 182.7, 149.9, 149.3, 143.6, 141.0, 140.4, 139.4, 126.2, 125.9, 124.0, 123.8, 123.3, 122.7, 120.6, 119.3, 117.7, 113.3, 109.2, 109.1, 105.4, 47.4, 43.2, 31.8, 31.4, 30.3, 29.4, 29.2, 29.0, 27.3, 26.7, 22.6, 22.5, 14.1, 14.0. HRMS (ESI, *m/z*): [M + H]$^+$ calcd for (C$_{35}$H$_{41}$N$_2$OS$_2$): 569.2655, found: 569.2623.

2.1.3. 4-[4-(Di-*p*-tolylamino)phenyl]-6-[4-(diphenylamino)phenyl]-4*H*-dithieno[3,2-*b*:2′,3′-*d*]pyrrole-2-carbaldehyde (5-T). A mixture of [4-(diphenylamino)phenyl]boronic acid (117 mg, 0.40 mmol), **3-T** (150 mg, 0.27 mmol), tetrakis(triphenylphosphine)palladium(0) (30 mg, 0.026 mmol), and potassium carbonate (2 M aqueous solution 1 mL, 2 mmol) in THF (25 mL) was stirred and heated to reflux under argon for 20 h. The reaction mixture was poured into water and extracted with DCM, and the combined extracts were washed with brine, dried over anhydrous MgSO$_4$, and filtered. The solvent was removed by rotary evaporation under vacuum, and the crude product was purified by column chromatography on silica gel, to give a yellow solid in 89.9% (175 mg) yield. Mp 183–185 °C. ^{1}H NMR (CDCl$_3$, 400 MHz, ppm): δ 9.83 (s, 1H), 7.72 (s, 1H), 7.50–7.48 (m, 2H), 7.37–7.35 (m, 2H), 7.30–7.28 (m, 3H), 7.24 (s, 1H), 7.17–7.11 (m, 11H), 7.08–7.05 (m, 8H), 2.34 (s, 6H). ^{13}C NMR (CDCl$_3$, 100 MHz): δ ppm 182.8, 148.9, 148.1, 147.8, 147.5, 147.3, 144.9, 143.3, 140.1, 133.4, 131.7, 130.1, 129.4, 128.4, 126.6, 125.0, 124.9, 124.8, 124.0, 123.8, 123.5, 123.2, 122.7, 114.8, 106.7, 20.9. HRMS (ESI, *m/z*): [M + H]$^+$ calcd for (C$_{47}$H$_{36}$N$_3$OS$_2$): 722.2294, found: 722.2287.

2.1.4. 6-(4-(Diphenylamino)phenyl)-4-(4-methoxyphenyl)-4*H*-dithieno[3,2-*b*:2′,3′-*d*]pyrrole-2-carbaldehyde (5-P). Compound **5-P** was synthesized from **3-P** according to the same procedure as that of **5-T**, and was obtained as a yellow solid in 96.9% yield. Mp 115–117 °C. ^{1}H NMR (CDCl$_3$, 400 MHz, ppm): δ 9.82 (s, 1H), 7.66 (s, 1H), 7.50–7.47 (m, 4H), 7.30–7.28 (m, 3H),

7.18 (s, 1H), 7.14–7.05 (m, 11H), 3.90 (s, 3H). ^{13}C NMR (CDCl$_3$, 100 MHz): δ ppm 182.8, 158.7, 149.1, 148.1, 147.9, 147.2, 143.5, 140.2, 131.7, 129.4, 128.3, 126.6, 124.8, 123.5, 123.1, 122.6, 120.3, 115.2, 114.8, 106.5, 55.7. HRMS (ESI, m/z): [M + H]$^+$ calcd for (C$_{34}$H$_{25}$N$_2$O$_2$S$_2$): 557.1352, found: 557.1351.

2.1.5. (E)-2-Cyano-3-{4-[4-(di-p-tolylamino)phenyl]-4H-dithieno[3,2-b:2′,3′-d]pyrrol-2-yl}acrylic acid (DT). Compound **2-T** (200 mg, 0.418 mmol) was dissolved in 30 mL of chloroform and cyanoacetic acid (140 mg, 1.672 mmol), and the mixture was refluxed in the presence of piperidine (0.1 mL) for 20 h under argon. After cooling, the reaction mixture was poured into water (30 mL) and extracted with DCM. The combined organic phases were dried over anhydrous MgSO$_4$, and the solvent was evaporated under reduced pressure. The pure product was obtained using column chromatography on silica gel (CH$_2$Cl$_2$: MeOH = 20 : 1 as eluent) as an orange powder in 87.8% (200 mg) yield. Mp 243–245 °C. ^{1}H NMR (DMSO-d_6, 400 MHz): δ ppm 8.52 (s, 1H), 8.18 (s, 1H), 7.75–7.74 (m, 1H), 7.53–7.51 (m, 2H), 7.30–7.28 (m, 1H), 7.17–7.15 (m, 4H), 7.04–7.00 (m, 6H), 2.29 (s, 6H). ^{13}C NMR (DMSO-d_6, 100 MHz): δ ppm 164.1, 147.9, 146.4, 144.4, 142.9, 133.3, 132.9, 131.3, 131.2, 130.2, 124.9, 124.8, 123.6, 122.0, 117.3, 116.2, 112.3, 20.4. HRMS (ESI, m/z): [M]$^+$ calcd for (C$_{32}$H$_{23}$N$_3$O$_2$S$_2$): 545.1226, found: 545.1209.

2.1.6. (E)-2-Cyano-3-(4-(4-(di-p-tolylamino)phenyl)-6-(9-octyl-9H-carb-azol-3-yl)-4H-dithieno[3,2-b:2′,3′-d]pyrrol-2-yl)acrylic acid (CD-T). Compound **CD-T** was synthesized from **4-T** according to the same procedure as that of **DT**, and was obtained as a brown power in 85.3% yield. Mp 256–258 °C. ^{1}H NMR (DMSO-d_6, 400 MHz, ppm): δ 13.4 (s, 1H), 8.61 (m, 1H), 8.52 (s, 1H), 8.25 (d, J = 8 Hz, 1H), 8.16 (s, 1H), 7.83–7.81 (m, 1H), 7.74 (s, 1H), 7.63–7.59 (m, 4H), 7.50–7.46 (m, 1H), 7.24–7.21 (m, 1H), 7.19–7.17 (m, 4H), 7.08–7.03 (m, 6H), 4.39 (t, J = 6.4 Hz, 2H), 2.30 (s, 6H), 1.78–1.75 (m, 2H), 1.25–1.17 (m, 10H), 0.82–0.79 (m, 3H). ^{13}C NMR (DMSO-d_6, 100 MHz): δ ppm 164.3, 149.8, 148.8, 148.0, 146.5, 144.4, 142.5, 140.6, 140.1, 133.0, 132.8, 131.1, 130.2, 126.2, 125.7, 125.2, 124.9, 123.8, 123.7, 122.6, 122.0, 121.9, 120.8, 119.1, 117.5, 117.3, 114.3, 109.8, 109.6, 107.1, 93.6, 42.3, 31.1, 28.7, 28.6, 28.5, 26.4, 22.0, 20.4, 13.9. HRMS (ESI, m/z): [M]$^+$ calcd for (C$_{52}$H$_{46}$N$_4$O$_2$S$_2$): 822.3057, found: 822.3030.

2.1.7. (E)-2-Cyano-3-[4-hexyl-6-(9-octyl-9H-carbazol-3-yl)-4H-dithieno[3,2-b:2′,3′-d]pyrrol-2-yl]acrylic acid (CD-C). Compound **CD-C** was synthesized from **4-C** according to the same procedure as that of **DT**, and was obtained as a brown power in 74.8% yield. Mp 122–123 °C. ^{1}H NMR (DMSO-d_6, 400 MHz, ppm): δ 13.3 (s, 1H), 8.56–8.55 (m, 1H), 8.45 (s, 1H), 8.25 (d, J = 7.6 Hz, 1H), 8.13 (s, 1H), 7.84 (s, 1H), 7.82–7.80 (m, 1H), 7.64–7.59 (m, 2H), 7.50–7.46 (m, 1H), 7.26–7.22 (m, 1H), 4.38 (t, J = 6.8 Hz, 2H), 4.32 (t, J = 6.8 Hz, 2H), 1.88–1.85 (m, 2H), 1.77–1.74 (m, 2H), 1.28–1.15 (m, 16H), 0.83–0.78 (m, 6H). ^{13}C NMR (DMSO-d_6, 100 MHz): δ ppm 164.5, 150.7, 149.3, 147.8, 143.6, 140.6, 140.0, 132.0, 126.2, 125.4, 124.5, 123.6, 122.6, 122.0, 120.6, 119.1, 117.4, 117.2, 112.6, 109.9, 109.6, 106.7, 92.7, 46.7, 42.3, 31.1, 30.7, 30.6, 29.5, 28.7, 28.6, 28.5, 26.4, 25.9, 22.0, 13.9, 13.8. HRMS (ESI, m/z): [M]$^+$ calcd for (C$_{38}$H$_{41}$N$_3$O$_2$S$_2$): 635.2635, found: 635.2610.

2.1.8. (E)-2-Cyano-3-{4-[4-(di-p-tolylamino)phenyl]-6-[4-(di-phenylamino)phenyl]-4H-dithieno[3,2-b:2′,3′-d]pyrrol-2-yl}acrylic

acid (TD-T). Compound **TD-T** was synthesized from **5-T** according to the same procedure as that of **DT**, and was obtained as a black power in 88.9% yield. Mp 222–224 °C. ^{1}H NMR (DMSO-d_6, 400 MHz, ppm): δ 8.50 (s, 1H), 8.14 (s, 1H), 7.64–7.62 (m, 2H), 7.57 (s, 1H), 7.54–7.52 (m, 2H), 7.35–7.31 (m, 4H), 7.16–6.94 (m, 18H), 2.27 (s, 6H). ^{13}C NMR (DMSO-d_6, 100 MHz): δ ppm 164.3, 148.5, 147.8, 147.4, 146.6, 146.4, 144.3, 142.6, 133.1, 132.9, 131.0, 130.2, 129.6, 127.8, 126.6, 125.6, 124.8, 124.5, 123.7, 123.6, 122.4, 121.9, 117.2, 114.7, 107.4, 93.9, 20.4. HRMS (ESI, m/z): [M]$^+$ calcd for (C$_{50}$H$_{36}$N$_4$O$_2$S$_2$): 788.2274, found: 788.2255.

2.1.9. (E)-2-Cyano-3-{6-[4-(diphenylamino)phenyl]-4-(4-meth-oxyphenyl)-4H-dithieno[3,2-b:2′,3′-d]pyrrol-2-yl}acrylic acid (TD-P). Compound **TD-P** was synthesized from **5-P** according to the same procedure as that of **DT**, and was obtained as a brown power in 89.2% yield. Mp 187–189 °C. ^{1}H NMR (DMSO-d_6, 400 MHz, ppm): δ 13.4 (s, 1H), 8.48 (s, 1H), 8.08 (s, 1H), 7.65–7.61 (m, 4H), 7.52 (s, 1H), 7.35–7.31 (m, 4H), 7.17–7.15 (m, 2H), 7.12–7.05 (m, 6H), 6.97–6.95 (m, 2H), 3.85 (s, 3H). ^{13}C NMR (DMSO-d_6, 100 MHz): δ ppm 164.2, 158.1, 148.9, 147.9, 147.8, 147.5, 146.6, 143.0, 133.1, 130.8, 129.6, 127.8, 126.6, 125.4, 124.6, 124.5, 123.7, 123.2, 122.4, 117.3, 115.2, 114.5, 107.2, 93.9, 55.5. HRMS (ESI, m/z): [M]$^+$ calcd for (C$_{37}$H$_{25}$N$_3$O$_3$S$_2$): 623.1332, found: 623.1316.

2.2. Measurement and characterization

^{1}H and ^{13}C NMR spectra were recorded on a Bruker 400 MHz spectrometer in CDCl$_3$ or DMSO-d_6 with tetramethylsilane as the inner reference. The melting points were taken on a Tektronix X4 microscopic melting point apparatus and were uncorrected. The absorption and emission spectra of the dyes in tetrahydrofuran solution (2×10^{-5} M) were measured at room temperature on a Shimadzu UV-2450 UV-Vis spectrophotometer and Fluorolog III photoluminescence spectrometer, respectively. Electrochemical redox potentials were measured using Cyclic Voltammetry (CV), with three electrode cells and an Ingsens 1030 electrochemical workstation (Ingsens Instrument Guangzhou, Co. Ltd., China) in one compartment at a scan rate of 50 mV s^{-1}. Ag/AgCl electrode in KCl (3 M) solution and an auxiliary platinum wire were utilized as reference and counter electrodes, respectively, while dye-coated TiO$_2$ films were used as the working electrodes. Tetrabutylammonium perchlorate (n-Bu$_4$NClO$_4$) 0.1 M in THF was used as the supporting electrolyte. All electrochemical measurements were calibrated by using ferrocene as a standard (0.63 V $vs.$ NHE). The current voltage characteristics were recorded using a Keithley 2400 source meter under simulated AM 1.5 G (100 mW cm^{-2}) illumination with a solar light simulator (Pecell-L15). A 1000 W xenon arc lamp (Oriel, Model: 6271) served as a light source and its incident light intensity was calibrated with a BS-520 standard Si solar cell. The incident monochromatic photon-to-current conversion efficiency (IPCE) spectra were measured as a function of wavelength from 350 to 800 nm using a PEC-S20 action spectrum measurement system. The electrochemical impedance spectra (EIS) measurements were conducted on an electrochemical workstation (Zahner Zennium) under dark conditions, with an applied bias potential of −0.8 V. A 10 mV AC sinusoidal signal was employed over the constant bias with the

frequency ranging between 1 MHz and 0.1 Hz. The impedance parameters were determined by fitting the impedance spectra using Z-view software. The amount of dye loaded was measured by desorbing the dye from the films with 0.1 M NaOH in THF/ H_2O (1 : 1) and measuring the UV-Vis spectrum.

2.3. Fabrication of DSSCs

A TiO_2 (anatase) film (∼12 μm in thickness) with a scattering layer (∼4 μm) was prepared according to a previous procedure.[43] The active area of the TiO_2 film was 0.4×0.4 cm^{-2}. The TiO_2 electrodes were immersed in a solution of the dyes for 16 h in the dark (0.5 mM dye in DCM/THF (1 : 1)). The dye-adsorbed TiO_2 films were washed with THF and dried. The dye-sensitized TiO_2/FTO photoanodes and Pt/FTO counter electrodes were assembled into sandwich-type solar cells. The electrolyte (0.6 M 1-methyl-3-propylimidazolium iodide (PMII), 0.1 M guanidinium thiocyanate, 0.07 M I_2, 0.05 M LiI, and 0.5 M tert-butylpyridine in acetonitrile) was injected into the seam between the two electrodes.

3. Results and discussion

3.1. Synthesis and characterization

The synthetic route to the five dyes containing the **DTP** moiety, i.e., **DT**, **CD-T**, **TD-T**, **CD-C** and **TD-P**, is depicted in Scheme 1. The starting materials **1-X**, **2-X** and **3-X** were synthesized according to our previous report.[44] The subsequent Suzuki–Miyaura cross-coupling reaction of 9-octyl-3-(4,4,5,5-tetramethyl-1,3,2-dioxaborolan-2-yl)-9H-carbazole with **3-X**, under modified conditions and tetrakis(triphenylphosphine)-palladium(0) as the catalyst precursor in a biphasic mixture of aqueous Na_2CO_3 and THF, afforded the corresponding

aldehyde **4-X** in yields of 68.7% and 91.9%, respectively. The same procedure was applied for the preparation of **5-X** from a reaction of **3-X** and [4-(diphenylamino)phenyl]-boronic acid. The target products were then obtained by the reaction of the corresponding precursors with cyanoacetic acid via the Knoevenagel condensation reaction in the presence of piperidine to yield **CD-C**, **CD-T**, **TD-T** and **TD-P** (74.8–89.2%). The structures of the new compounds were confirmed by ^{1}H NMR, ^{13}C NMR and HRMS spectra.

3.2. Absorption properties in solution

The UV-Vis absorption spectra of the organic dyes **DT**, **CD-T**, **TD-T**, **CD-C** and **TD-P** in CH_2Cl_2/THF (1 : 1) solution are displayed in Fig. 2 and the parameters are listed in Table 1. Each of these dyes exhibited two major distinct absorption bands at 300–350 nm and 400–550 nm. The former is ascribed to a localized aromatic π–π* transition and the latter exhibits intramolecular charge-transfer (ICT) characteristics.[45] The absorption maxima (ICT) for **DT**, **CD-T**, **TD-T**, **CD-C** and **TD-P** in solution are 436 nm, 492 nm, 492 nm, 496 nm and 493 nm in the visible region, respectively, indicating that the donor unit at the 6-position of **DTP** ring can lead to a better absorption performance compared to the donor unit at the 4-position (N-atom) of **DTP** ring. Except for **DT**, the spectra of **CD-T**, **TD-T**, **CD-C** and **TD-P** are quite similar, but the molar extinction coefficients (ε) of **TD-T** (ε = 44 555 M^{-1} cm^{-1}) and **TD-P** (ε = 49 945 M^{-1} cm^{-1}) are smaller than those of **CD-T** (ε = 56 370 M^{-1} cm^{-1}) and **CD-C** (ε = 62 471 M^{-1} cm^{-1}), which indicates the superiority of the carbazole donor in its light harvesting capability. When a triphenylamine group was attached to the nitrogen atom of the **DTP** ring, the absorption ranges of **CD-T** and **TD-T** show slight narrowing and the molar
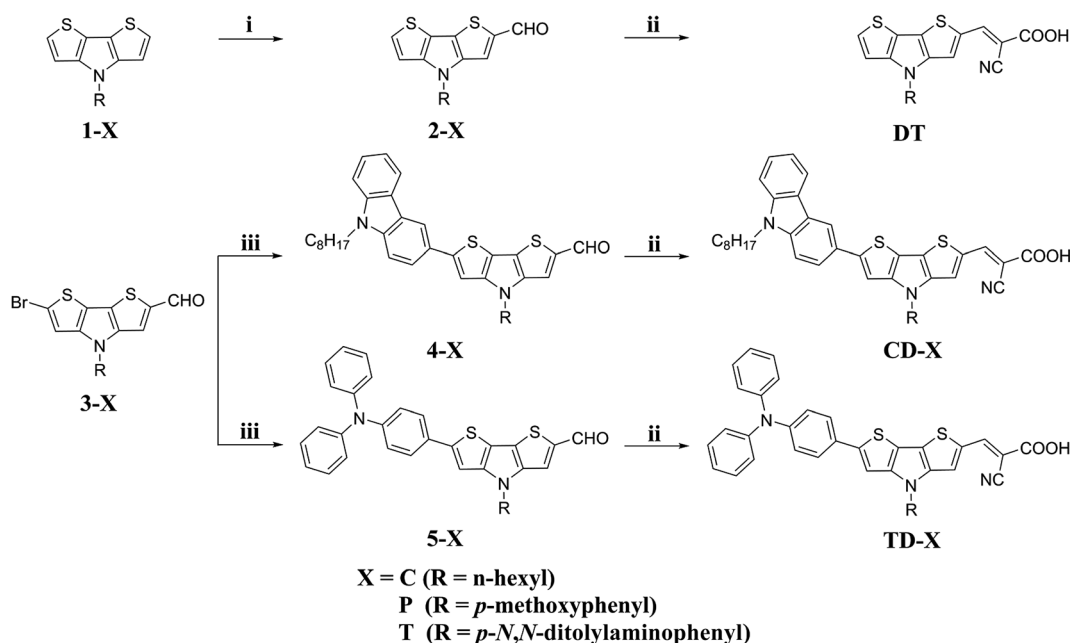
Scheme 1 Synthetic route for the target dyes: (i) DMF, POCl₃, 1,2-dichloroethane, 40 °C, 4 h; (ii) cyanoacetic acid, piperidine, CHCl₃, reflux, 20 h; (iii) Pd(PPh₃)₄, K₂CO₃, THF, 80 °C, 20 h.

Table 1 Band gap (calculated by DFT/B3LYP), absorption, and electrochemical parameters for organic dyes[a]

Dye	(HOMO/LUMO)[b] /eV	Band gap[b]	$(\lambda_{abs}{}^c/nm)/(\varepsilon/M^{-1}\,cm^{-1})$	HOMO[d] (vs. NHE)/V	$E_{0\text{-}0}$/eV	LUMO[e] (vs. NHE)/V
DT	−5.19/−2.45	2.74	436(43 200)	0.51(−5.26)	2.84	−2.42
CD-T	−5.07/−2.35	2.72	492(56 370)	0.79(−5.54)	2.52	−3.02
TD-T	−4.97/−2.41	2.56	492(44 555)	0.52(−5.27)	2.52	−2.75
CD-C	−5.10/−2.37	2.73	496(62 471)	0.60(−5.35)	2.50	−2.85
TD-P	−4.98/−2.43	2.55	493(49 945)	0.71(−5.46)	2.52	−2.94

[a] ε: absorption coefficient; $E_{0\text{-}0}$: 0-0 transition energy measured at the onset of absorption spectra. [b] DFT/B3LYP calculated values. [c] Absorptions due to charge-transfer transitions were measured in CH_2Cl_2/THF (1 : 1). [d] HOMO of dyes measured using cyclic voltammetry in 0.1 M tetrabutylammonium perchlorate in THF solution as supporting electrolyte, Ag/AgCl as reference electrode and Pt as counter electrode. [e] LUMO was calculated by HOMO − $E_{0\text{-}0}$.
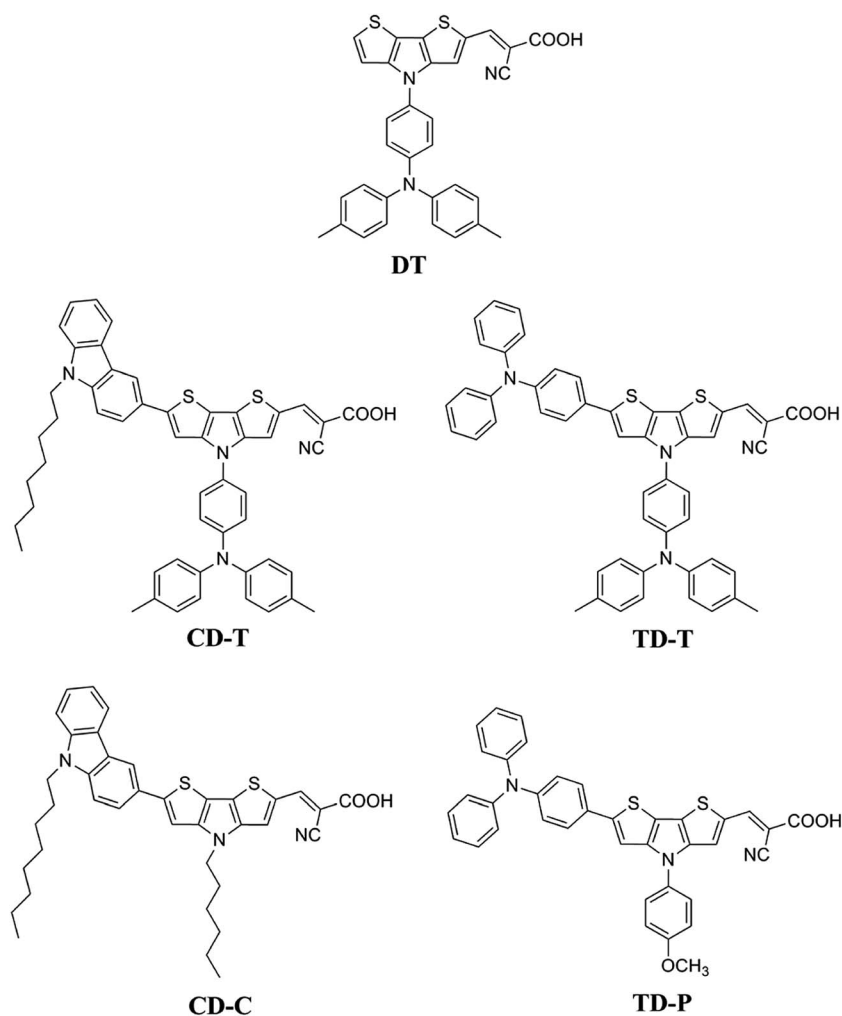

Fig. 1 Structures of the DTP-based dyes DT, CD-T, TD-T, CD-C and TD-P.

extinction coefficients are obviously decreased compared with those of **CD-C** and **TD-P** (see Fig. 1), which is consistent with our previous report.[44]

3.3. Electrochemical properties

To study the redox potentials of all the dyes (**DT, CD-T, TD-T, CD-C** and **TD-P**) and their energy levels, the electrochemical behaviors were studied using cyclic voltammetry (CV) in THF solution (Fig. 3). Quasi-reversible oxidation waves (E_{ox}) were used to estimate the highest occupied molecular orbital (HOMO) energies, whereas quasi-reversible reduction waves (E_{red}) were used to estimate the lowest unoccupied molecular orbital (LUMO) energies. As shown in Table 1, all the five dyes exhibit more negative LUMO levels (−2.33, −1.73, −2.00, −1.90
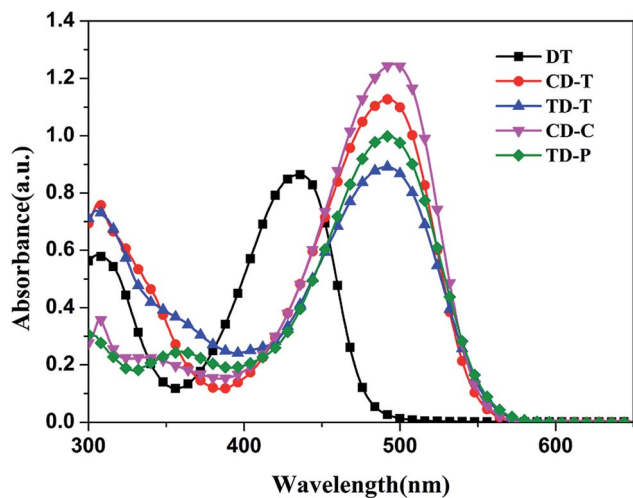
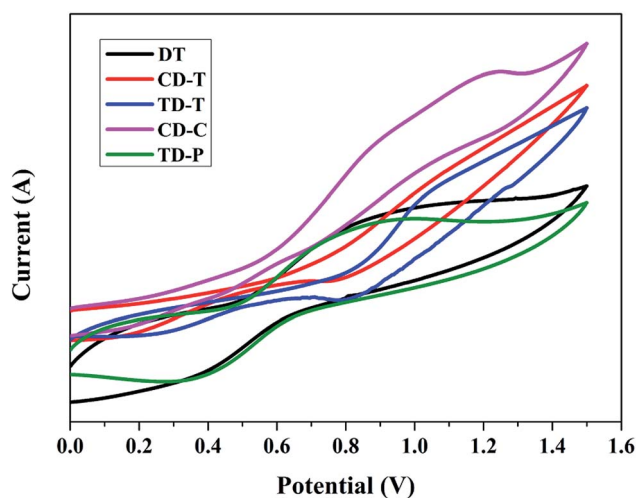Fig. 2 UV-Vis spectra of the sensitizers in CH_2Cl_2/THF (1 : 1) solution.

Fig. 3 Cyclic voltammograms of the dye-loaded TiO_2 films.

and −1.81 V) than the conductive band of TiO_2 (−0.5 V *vs.* NHE), indicating that the electron injection process is energetically permitted. The first oxidation potentials, corresponding to the HOMO energy levels of sensitizers **DT**, **CD-T**, **TD-T**, **CD-C** and **TD-P**, were determined to be 0.51, 0.79, 0.52, 0.60 and 0.71 V, respectively, which are more positive than the I^-/I_3^- redox couple (0.4 V *vs.* NHE), providing a thermodynamic driving force for efficient dye regeneration. The zero–zero band gaps (E_{0-0}), estimated from the onset of the UV-Vis absorption spectra, were in the range of 2.50–2.84 eV.

3.4. Molecular calculations

To obtain further insight into the geometrical and electronic distribution of these dyes, density functional theory (DFT) calculations were performed at the B3LYP/6-31G* level. The ground-state structures of the five dyes are shown in Fig. 4. As can be easily seen, the dihedral angles of the carbazole-dithienopyrrole moiety in the optimized structures of **CD-C**

and **CD-T** are 30.3° and 26.9°, respectively, while the dihedral angles of the triphenylamine-dithienopyrrole moiety in the dyes of **TD-P** and **TD-T** are 23.8° and 24.5°, respectively, indicating that the bulky triphenylamine groups attached to the **DTP** ring do not twist the conjugation system. Thus, this configuration not only maintains charge transfer through the whole conjugation system, but also prevents π–π* stacking between the planar structures. The torsional angle between the phenyl group on the side chain and the **DTP** plane in **DT** is 48.5°. For **CD-T**, **TD-T** and **TD-P**, the torsional angles of the corresponding units are 48°, 49.3° and 51.7°, respectively. As the dihedral angles between these two aromatic units are relatively large, conjugation between the side chains and the **DTP** rings is disrupted. This disruption of the conjugation is reflected in the experimental optical spectra of the chromophores in **CD-C** and **CD-T**, which have almost the same absorption range.

The energies and the electronic distributions of the frontier molecular orbitals (HOMOs and LUMOs) of the dyes computed are presented in Fig. 5. The electron distributions of the HOMO and LUMO of **CD-T**, **TD-T**, **CD-C** and **TD-P** are similar. The HOMO levels of these dye molecules are mainly dominated by a π-orbital contribution of the triphenylamine or carbazole donor with a small contribution from the **DTP** ring π-orbital. Meanwhile, the LUMO levels are delocalized through the **DTP** units and cyanoacrylic acid fragments, with a sizable contribution from the latter. It is also worthwhile to note that in the optimized structure of the dye **DT**, the HOMO level is delocalized over the triphenylamine group attached to the N-atom of the **DTP** ring, but there is nearly no electron distribution of the HOMO on the **DTP** substituents in other dyes.

3.5. Adsorption amount

The amount of the dye adsorbed on the TiO_2 film (12 μm) was measured by dipping the films into a 0.1 M aqueous solution of NaOH/THF (1 : 1) and measuring the absorbance of the desorbed dye solution. As listed in Table 2, the amounts of dye absorbed on the TiO_2 films were 2.97, 3.03, 3.79, 4.05 and 5.74 × 10^{-7} mol cm^{-2} for **DT**, **CD-T**, **TD-T**, **CD-C** and **TD-P**, respectively. Compared with **CD-C** and **TD-P**, the **TPA**-substituted **DT**, **CD-T** and **TD-T** showed lower uptake, which may be due to the bulky groups on the side chain, leading to weak electronic coupling with nanoporous TiO_2 and hence, decreased dye uptake. This is also the reason why the **DT** dye-sensitized cell showed the lowest current density (7.09 mA cm^{-2}). In addition, the dye adsorption amount of **TD-P** was higher than that of **CD-C**, which indicates that the incorporation of appropriate size groups in the side chain not only inhibits the π–π aggregation of dye molecules, but also does not cause a decrease in molecular adsorption.

3.6. Photovoltaic properties of the DSSCs

The incident monochromatic photo-to-current conversion efficiency (IPCE) as a function of incident wavelength for DSSCs based on the dyes using a liquid electrolyte is shown in Fig. 6a. These results are in good agreement with the UV-Vis absorption results (Fig. 1), and the IPCE action spectra for the DSSC based
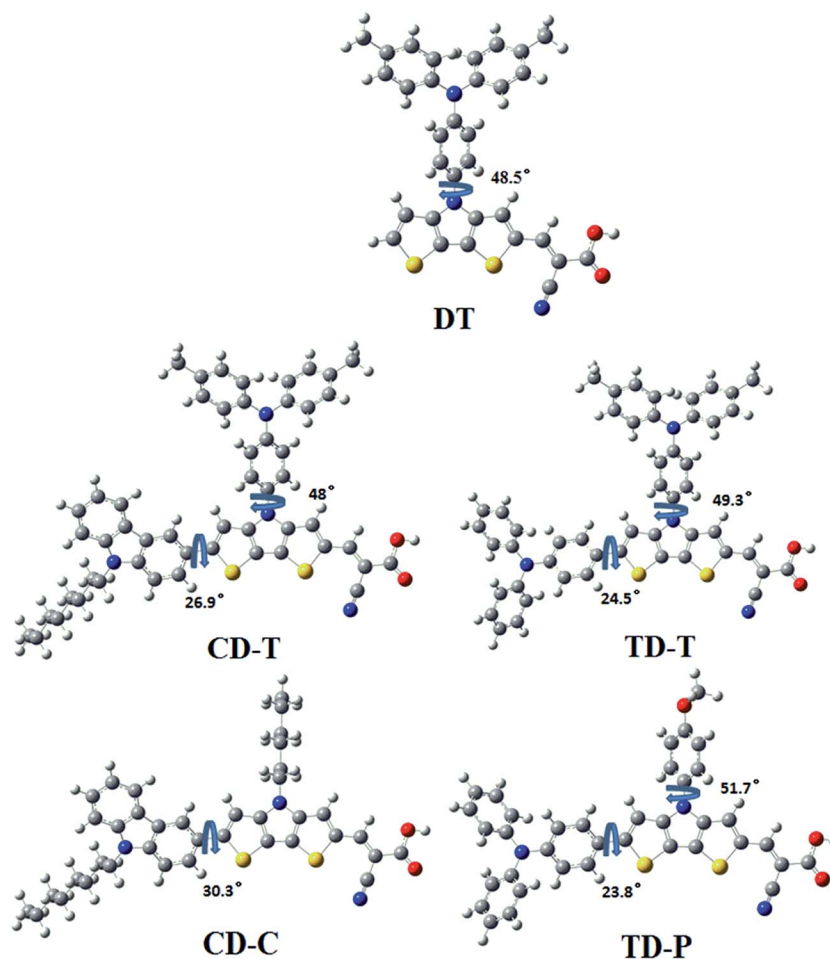
Fig. 4 Optimized ground state geometry and related dihedral angels for the sensitizers DT, CD-T, TD-T, CD-C and TD-P.
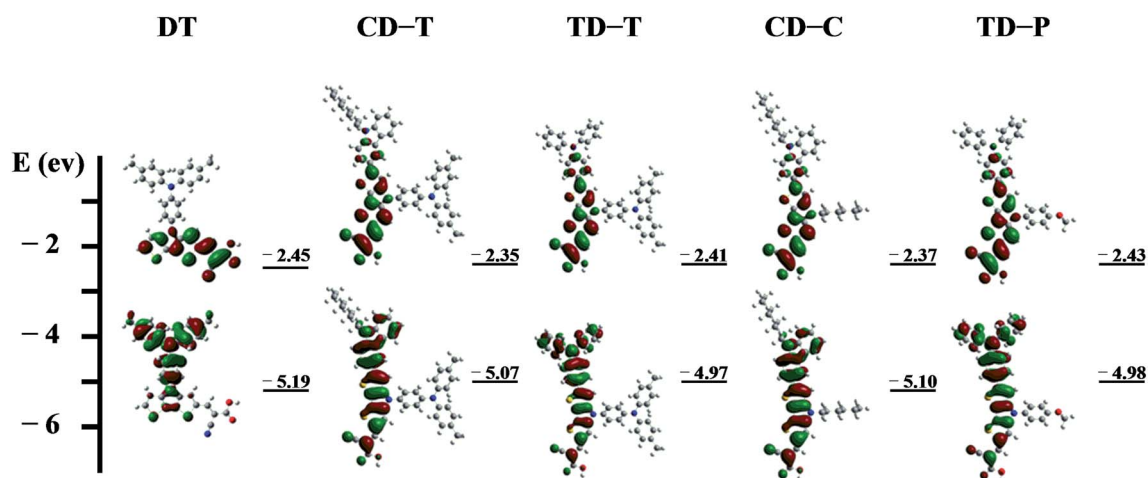

**Fig. 5** Frontier orbitals of the sensitizers plotted at an isosurface value of 0.02.

on **DT** is narrower than for the DSSCs based on the others. It is evident that all five dyes can efficiently convert visible light into photocurrent in the region from 400 nm to 700 nm. The IPCE exceeds 60% in the range of 410–580 nm for **CD-T**, 450–530 nm for **TD-T**, 420–580 nm for **CD-C** and 410–580 nm for **TD-P**, with the highest value of 69.3% at 490 nm for **CD-T**, 63.1% at 490 nm for **TD-T**, 66.2% at 510 nm for **CD-C** and 66.3% at 490 nm for **TD-P**. However, the highest value of IPCE for **DT** was only 52.9%

Table 2 Photovoltaic parameters for DSSCs of organic dyes

Dye	J_{sc} (mA cm^{-2})	V_{oc} (mV)	FF	η (%)	Amount of dye load (mol cm^{-2})
DT	7.09	0.62	0.79	3.68	2.97×10^{-7}
CD-T	14.55	0.71	0.64	6.63	3.03×10^{-7}
TD-T	13.39	0.69	0.65	5.96	3.79×10^{-7}
CD-C	14.71	0.70	0.63	6.50	4.05×10^{-7}
TD-P	14.79	0.72	0.61	6.44	5.74×10^{-7}
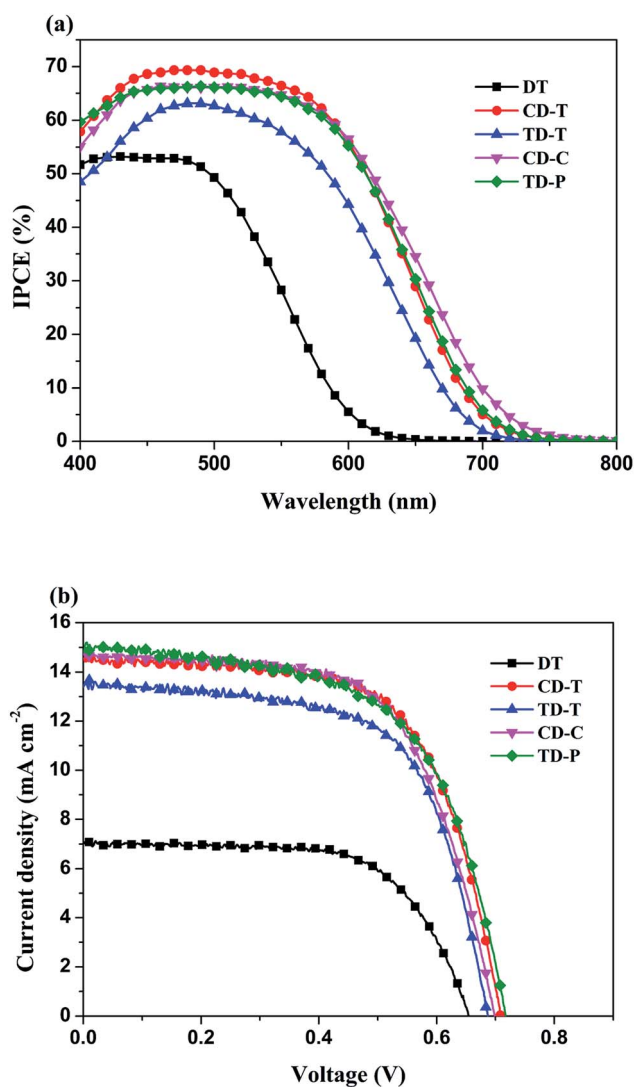
Fig. 6 (a) IPCE action spectra and (b) current-density–voltage (J–V) curves for the DSSCs based on DT, CD-T, TD-T, CD-C and TD-P.

at 470 nm. The differences in the maximum IPCE values arise from three factors, *i.e.*, the difference between the LUMO and the conduction band edge, the absorption capacity (Fig. 1 and Table 1), and the amount of dye adsorbed on the TiO$_2$ film.[45–47] Among these five dyes, it can be easily seen that the IPCE for **DT** displayed the poorest performance with low IPCE values and narrow IPCE spectra, while the IPCE for **CD-T** exhibited the best

performance with high IPCE values over a broad spectral region, indicating that a **CD-T**-sensitized TiO$_2$ electrode would generate a higher conversion yield compared to those of the other four dyes. The IPCE values of **CD-T**, based on the carbazole donor, are obviously higher than those of **TD-T**, based on triphenylamine donor, which may be a result of the high molar extinction coefficient. Generally, a high molar extinction coefficient means a good light harvesting ability, suggesting that the dye would convert light to electricity more efficiently.[48] Thus, the high molar extinction coefficients would allow the carbazole donor dye to display good IPCE performance. On the other hand, although **TD-T** has almost the same IPCE spectrum as **TD-P**, the IPCE performance of the **TD-P** device is much higher than that of the **TD-T** device. Consistent with the absorption spectra of the dyes in solution, the higher IPCE values for the **TD-P**-based DSSC may also be attributed to its higher absorption. The relatively higher IPCE of the **TD-P**-based cell may lead to a higher short-circuit photocurrent density compared with that of **TD-T**.

The photocurrent–voltage (I–V) plots of the DSSCs fabricated with these dyes are shown in Fig. 6b. The detailed parameters, *i.e.*, short circuit current (J_{sc}), open-circuit photovoltage (V_{oc}), fill factor (FF), and solar-to-electrical energy conversion efficiency (η) measured under AM 1.5 solar light (100 mW cm^{-2}) are summarized in Table 2.

As compared in Table 2 and Fig. 6, the overall efficiencies of the DTP-sensitized DSSCs follow the order: **CD-T** > **CD-C** > **TD-P** > **TD-T** > **DT**. The superior performance of the **CD-T**, **CD-C** and **TD-P** cells can be understood *via* their better photovoltaic characteristics. The J_{sc}, V_{oc}, and FF values of the **CD-T**, **CD-C** and **TD-P** cells are (14.55 mA cm^{-2}, 0.71 mV, 0.64), (14.71 mA cm^{-2}, 0.70 mV, 0.63) and (14.79 mA cm^{-2}, 0.72 mV, 0.61), respectively, yielding higher overall efficiencies of 6.63%, 6.50% and 6.44%, respectively. In contrast, **TD-T** and **DT** show poorer J_{sc}, V_{oc}, and FF values of (13.39 mA cm^{-2}, 0.69 mV, 0.65) and (7.09 mA cm^{-2}, 0.62 mV, 0.79), respectively, leading to inferior conversion efficiencies of 5.96% and 3.68%, respectively. There are two major structural factors worthy of attention: (1) the effects of different donor groups and (2) the influence induced by the substituent at the N-atom of the **DTP** ring.

Adding a substituent at the N-atom of the **DTP** ring seems to have a beneficial effect. It was found that the V_{oc} increases from 0.70 to 0.71 mV when the substituent was changed from the hexyl (**CD-C**) to the **TPA** (**CD-T**) unit. This was assigned to the reduced recombination ability at the TiO$_2$/dye/electrolyte interface by insulating the bulky phenyl groups on the dyes.

A similar result can also be detected in the Bode plot. The higher frequency peak (>100 Hz in Fig. 7a) represents the electron transfer processes at the Pt/electrolyte interface, while the lower frequency peak (<100 Hz) represents the electron transfer processes at the TiO$_2$/dye/electrolyte interface. From Fig. 7a it is clear that the positions of the high-frequency peaks for the two dyes did not change much, but the low-frequency peaks show a significant difference.

3.7. Electrochemical impedance spectroscopy analysis

Electrochemical impedance spectroscopy (EIS) analysis was employed to investigate the transfer and suppression of
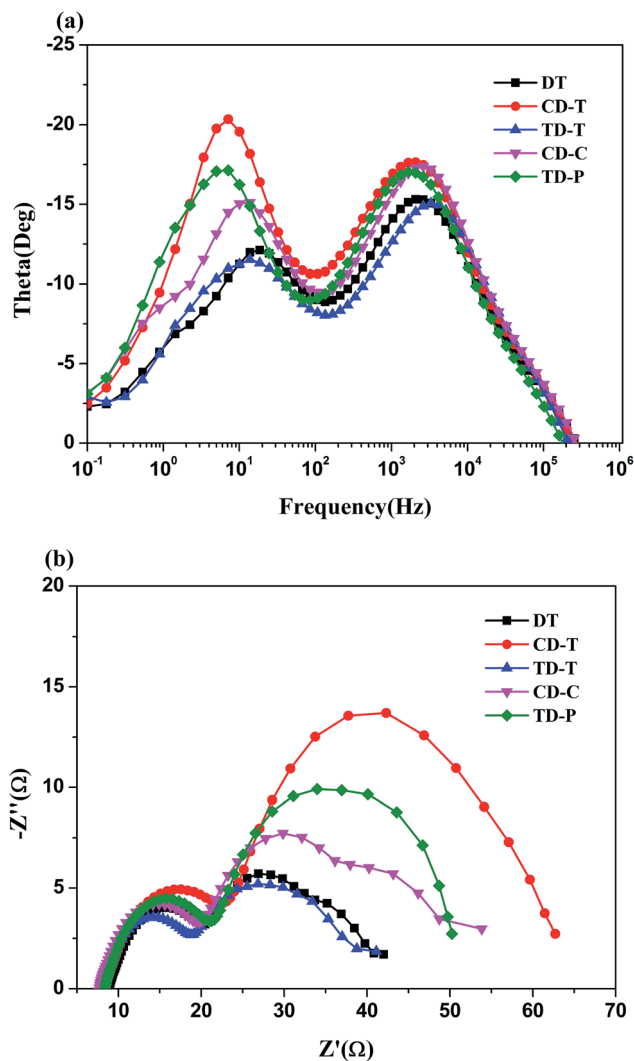
Fig. 7 (a) EIS Bode plots and (b) EIS Nyquist plots for DSSCs based on the five sensitizers measured in the dark under −0.8 V bias.

electrons in the DSSCs. The Nyquist plots for the DSSCs based on the dyes under a forward bias of −0.8 V in the dark with a frequency range of 0.1 Hz to 10^6 Hz are displayed in Fig. 7b. The five sensitizers all exhibit two semicircles. The first semicircle (R_{ce}) is assigned to charge transfer at the Pt/electrolyte interface, while the larger semicircle (R_{rec}) at lower frequencies relates to the charge transfer at the TiO$_2$/dye/electrolyte interface.[49,50] Obviously, the radius of the large semicircle increased in the order of **TD-T** < **DT** < **CD-C** < **TD-P** < **CD-T**, indicating that the **CD-T**-based device had the largest R_{rec}. In the Bode phase plots (Fig. 7a), the peak with the middle frequency is related to the electron lifetime, while the lower frequency peak corresponds to a longer electron lifetime. The electron lifetime (τ_r) can be estimated from $\tau_r = 1/(2\pi f_{max})$, where f_{max} is the peak frequency in lower frequency region.[51,52] As shown in Fig. 7a, the f_{max} value decreases in the order of **DT** (18.62 Hz) > **TD-T** (13.79 Hz) > **CD-C** (11.91 Hz) > **CD-T** (7.15 Hz) > **TD-P** (6.07 Hz). Thus, the electron lifetimes of the five dyes increase in the order of **DT** (8.5 ms) < **TD-T** (11.5 ms) < **CD-C** (13.4 ms) < **CD-T** (22.3 ms) <

TD-P (26.2 ms). A longer electron lifetime corresponds to a lower dark current. Thus, the DSSC based on **TD-P** has the highest V_{oc}. It is shown that triphenylamine used as an electron donor and the introduction of a benzene ring in the π-side chain are beneficial to the inhibition of electron recombination. However, the position and number of the benzene ring have a great influence on the electron lifetime.

4. Conclusion

In summary, five novel metal-free organic dyes containing a **DTP** unit as the π-spacer were successfully synthesized and utilized in DSSCs. In this study, we focused on the different effects of spatial structures and connection positions within the DSSCs. The results show that the smaller the dihedral angle between the donor unit and the bridging unit in the dye molecule, the higher the molar extinction coefficient of the molecule and the stronger the ability to capture light. In addition, the open circuit voltage (V_{oc}) was improved by attaching a benzene ring unit to the **DTP** unit (compared to an alkyl chain), which proved to be an effective strategy to reduce the π–π aggregation of the dyes on the TiO$_2$ films and suppress charge recombination. It is worth noting that the open-circuit photovoltage of the **TD-P** cell is superior to that of the **TD-T** cell. In addition, the dye adsorption amount of **TD-P** is also higher than that of **TD-T**, which indicates that the introduction of a suitable group in the side chain may lead to better results.

Acknowledgements

References

1 B. O'Regan and M. Grätzal, *Nature*, 1991, **353**, 737–740.
2 A. Hagfeldt, G. Boschloo, L. Sun, L. Kloo and H. Pettersson, *Chem. Rev.*, 2010, **110**, 6595–6663.
3 J. Yang, P. Ganesan, J. Teuscher, T. Moehl, Y. J. Kim, C. Yi, P. Comte, K. Pei, T. W. Holcombe, M. K. Nazeeruddin, J. Hua, S. M. Zakeeruddin, H. Tian and M. Grätzel, *J. Am. Chem. Soc.*, 2014, **136**, 5722–5730.
4 J. Mao, N. He, Z. Ning, Q. Zhang, F. Guo, L. Chen, W. Wu, J. Hua and H. Tian, *Angew. Chem., Int. Ed.*, 2012, **51**, 9873–9876.
5 S. D. Sousa, S. Lyu, L. Ducasse, T. Toupance and C. Olivier, *J. Mater. Chem. A*, 2015, **3**, 18256–18264.
6 P. Wang, C. Klein, R. Humphry-Baker, S. M. Zakeeruddin and M. Grätzel, *J. Am. Chem. Soc.*, 2005, **127**, 808–809.
7 Z. S. Wang and H. Sugihara, *Langmuir*, 2006, **22**, 9718–9722.
8 F. D. Angelis, S. Fantacci, A. Selloni, M. Grätzel and M. K. Nazeeruddin, *Nano Lett.*, 2007, **7**, 3189–3195.

9 S. Mori, M. Nagata, Y. Nakahata, K. Yasuta, R. Goto, M. Kimura and M. Taya, *J. Am. Chem. Soc.*, 2010, **132**, 4054–4055.

10 Y. Xie, Y. Tang, W. Wu, Y. Wang, J. Liu, X. Li, H. Tian and W. Zhu, *J. Am. Chem. Soc.*, 2015, **137**, 14055–14058.

11 S. Arrechea, J. N. Clifford, L. Pellejà, A. Aljarilla, P. d. l. Cruz, E. Palomares and F. Langa, *Dyes Pigm.*, 2016, **126**, 147–153.

12 C. Li, L. Luo, D. Wu, R. Jiang, J. Lan, R. Wang, L. Huang, S. Yang and J. You, *J. Mater. Chem. A*, 2016, **4**, 11829–11834.

13 J. Luo, J. Zhang, K. Huang, Q. Qi, S. Dong, J. Zhang, P. Wang and J. Wu, *J. Mater. Chem. A*, 2016, **4**, 8428–8434.

14 C. Yi, F. Giordano, N. Cevey-Ha, H. N. Tsao, S. M. Zakeeruddin and M. Grätzel, *ChemSusChem*, 2014, **7**, 1107–1113.

15 K. Kakiage, Y. Aoyama, T. Yano, K. Oya, J. Fujisawa and M. Hanaya, *Chem. Commun.*, 2015, **51**, 15894–15897.

16 T. Horiuchi, H. Miura and S. Uchida, *Chem. Commun.*, 2003, 3036–3037.

17 Z. Ning, Q. Zhang, W. Wu, H. Pei, B. Liu and H. Tian, *J. Org. Chem.*, 2008, **73**, 3791–3797.

18 H. Zhu, Y. Wu, J. Liu, W. Zhang, W. Wu and W. Zhu, *J. Mater. Chem. A*, 2015, **3**, 10603–10609.

19 D. P. Hagberg, T. Edvinsson, T. Marinado, G. Boschloo, A. Hagfeldt and L. Sun, *Chem. Commun.*, 2006, **21**, 2245–2247.

20 S. S. Park, Y. S. Won, Y. C. Choi and J. H. Kim, *Energy Fuels*, 2009, **23**, 3732–3736.

21 H.-Y. Yang, Y.-S. Yen, Y.-C. Hsu, H.-H. Chou and J. T. Lin, *Org. Lett.*, 2010, **12**, 16–19.

22 S. Paek, H. Choi, H. Choi, C.-W. Lee, M.-S. Kang, K. Song, M. K. Nazeeruddin and J. Ko, *J. Phys. Chem. C*, 2010, **114**, 14646–14653.

23 W. Li, Y. Wu, X. Li, Y. Xie and W. Zhu, *Energy Environ. Sci.*, 2011, **4**, 1830–1837.

24 J. Mao, N. He, Z. Ning, Q. Zhang, F. Guo, L. Chen, W. Wu, J. Hua and H. Tian, *Angew. Chem., Int. Ed.*, 2012, **51**, 9873–9876.

25 X. Ren, S. Jiang, M. Cha, G. Zhou and Z.-S. Wang, *Chem. Mater.*, 2012, **24**, 3493–3499.

26 L. Yang, Z. Zheng, Y. Li, W. Wu, H. Tian and Z. Wang, *Chem. Commun.*, 2015, **51**, 4842–4845.

27 K. Pei, Y. Wu, H. Li, Z. Geng, H. Tian and W. Zhu, *ACS Appl. Mater. Interfaces*, 2015, **7**, 5296–5304.

28 A. Shao, Y. Xie, S. Zhu, Z. Guo, S. Zhu, J. Guo, P. Shi, T. D. James, H. Tian and W. Zhu, *Angew. Chem., Int. Ed.*, 2015, **127**, 7383–7388.

29 N. Zhou, K. Prabakaran, B. Lee, S. H. Chang, B. Harutyunyan, P. Guo, M. R. Butler, A. Timalsina, M. J. Bedzyk, M. A. Ratner, S. Vegiraju, S. Yau, C. Wu, R. P. H. Chang, A. Facchetti, M. Chen and T. J. Marks, *J. Am. Chem. Soc.*, 2015, **137**, 4414–4423.

30 N. Kaneza, J. Zhang, H. Liu, P. S. Archana, Z. Shan, M. Vasiliu, S. H. Polansky, D. A. Dixon, R. E. Adams, R. H. Schmehl, A. Gupta and S. Pan, *J. Phys. Chem. C*, 2016, **120**, 9068–9080.

31 T. N. Murakami, N. Koumura, E. Yoshida, T. Funaki, S. Takano, M. Kimura and S. Mori, *Langmuir*, 2016, **32**, 1178–1183.

32 J. Yang, P. Ganesan, J. Teuscher, T. Moehl, Y. J. Kim, C. Yi, P. Comte, K. Pei, T. W. Holcombe, M. K. Nazeeruddin, J. Hua, S. M. Zakeeruddin, H. Tian and M. Grätzel, *J. Am. Chem. Soc.*, 2014, **136**, 5722–5730.

33 R. Y.-Y. Lin, F.-L. Wu, C.-H. Chang, H.-H. Chou, T.-M. Chuang, T.-C. Chu, C.-Y. Hsu, P.-W. Chen, K.-C. Ho, Y.-H. Lo and J. T. Lin, *J. Mater. Chem. A*, 2014, **2**, 3092–3101.

34 M. Wang, S.-J. Moon, M. Xu, K. Chittibabu, P. Wang, N.-L. Cevey-Ha, R. Humphry-Baker, S. M. Zakeeruddin and M. Grätzel, *Small*, 2010, **6**(2), 319–324.

35 G. Schulz, M. Löbert, I. Ata, M. Urdanpilleta, M. Lindén, A. Mishra and P. Bäuerle, *J. Mater. Chem. A*, 2015, **3**, 13738–13748.

36 Z. Wang, M. Liang, Y. Tan, L. Ouyang, Z. Sun and S. Xue, *J. Mater. Chem. A*, 2015, **3**, 4865–4874.

37 Z. Wang, H. Wang, M. Liang, Y. Tan, F. Cheng, Z. Sun and S. Xue, *ACS Appl. Mater. Interfaces*, 2014, **6**, 5768–5778.

38 Z. Wang, M. Liang, H. Wang, P. Wang, F. Cheng, Z. Sun and X. Song, *ChemSusChem*, 2014, **7**, 795–803.

39 Y. Wang, L. Yang, M. Xu, M. Zhang, Y. Cai, R. Li and P. Wang, *J. Phys. Chem. C*, 2014, **118**, 16441–16446.

40 N. Cai, J. Zhang, M. Xu, M. Zhang and P. Wang, *Adv. Funct. Mater.*, 2013, **23**, 3539–3547.

41 A. Gupta, M. M. A. Kelson, V. Armel and A. Bilic, *Tetrahedron*, 2014, **70**, 2141–2150.

42 I. R. Perera, A. Gupta, W. Xiang, T. Daeneke, U. Bach, R. A. Evans, C. A. Ohlin and L. Spiccia, *Phys. Chem. Chem. Phys.*, 2014, **16**, 12021–12028.

43 H. Zhang, J. Fan, Z. Iqbal, D.-B. Kuang, L. Wang, D. Cao and H. Meier, *Dyes Pigm.*, 2013, **99**, 74–81.

44 H. Zhang, J. Fan, Z. Iqbal, D.-B. Kuang, L. Wang, H. Meier and D. Cao, *Org. Electron.*, 2013, **14**, 2071–2081.

45 W. Wu, J. Zhang, H. Yang, B. Jin, Y. Hu, J. Hua, C. Jing, Y. Long and H. Tian, *J. Mater. Chem.*, 2012, **22**, 5382–5389.

46 A. Hagfeldt, G. Boschloo, L. Sun, L. Kloo and H. Pettersson, *Chem. Rev.*, 2010, **110**, 6595–6663.

47 K. Pei, Y. Wu, A. Islam, S. Zhu, L. Han, Z. Geng and W. Zhu, *J. Phys. Chem. C*, 2014, **118**, 16552–16561.

48 H. Chen, H. Huang, X. Huang, J. N. Clifford, A. Forneli, E. Palomares, X. Zheng, L. Zheng, X. Wang, P. Shen, B. Zhao and S. Tan, *J. Phys. Chem. C*, 2010, **114**, 3280–3286.

49 S. Cai, X. Hu, Z. Zhang, J. Su, X. Li, A. Islam, L. Han and H. Tian, *J. Mater. Chem. A*, 2013, **1**, 4763–4772.

50 D. Wang, W. Ying, X. Zhang, Y. Hu, W. Wu and J. Hua, *Dyes Pigm.*, 2015, **112**, 327–334.

51 K. Pei, Y. Wu, A. Islam, Q. Zhang, L. Han, H. Tian and W. Zhu, *ACS Appl. Mater. Interfaces*, 2013, **5**, 4986–4995.

52 Z.-S. Huang, X.-F. Zang, T. Hua, L. Wang, H. Meier and D. Cao, *ACS Appl. Mater. Interfaces*, 2015, **7**, 20418–20429.